Mechanical models of the effect of grain boundary sliding on creep and creep rupture

V. Tvergaard

Revue Phys. Appl. **23** (1988) 595-604 AVRIL **1988**, PAGE 595
Classification
Physics Abstracts
62.20 – 46.30

Mechanical models of the effect of grain boundary sliding on creep and creep rupture

V. Tvergaard

Department of Solid Mechanics, The Technical University of Denmark, Building 404, 2800 Lyngby, Denmark

(*Reçu le 15 juin 1987, accepté le 2 novembre 1987*)

RÉSUMÉ - L'influence du glissement aux joints des grains sur les propriétés mécaniques des matériaux soumis au fluage à haute température a été étudiée par de nombreux modèles. Certains se sont concentrés sur l'interaction entre le comportement visqueux linéaire des joints et le fluage en loi puissance des grains. On trouve qu'il y a une zone de transition entre les fortes contraintes où le glissement au joint à peu d'influence et les faibles contraintes où il accélère le fluage. D'autres modèles se sont concentrés sur l'effet de glissement sur la rupture intergranulaire par fluage. Des joints de grains qui glissent facilement conduisent à des temps de rupture très courts, et le comportement est fortement influencé par la densité de facettes induisant la cavitation dans les joints de grains.

ABSTRACT - The influence of grain boundary sliding on the mechanical behaviour of materials subject to creep at elevated temperatures has been investigated by a number of model analyses. Some models have focussed on the interaction of linearly viscous behaviour in the grain boundaries and power-law creep of the grains. It is found that there is a transition range such that at higher stresses sliding has little influence, while at lower stresses sliding accelerates creep. Other investigations have focussed on the effect of sliding on intergranular creep fracture. Freely sliding grain boundaries give much reduced rupture times, and the behaviour is rather strongly affected by whether the cavitating grain boundary facets are closely-spaced or well-separated.

1. INTRODUCTION

A number of experiments on polycrystalline metals have demonstrated that the resistance to sliding on the grain boundaries is low compared to the resistance towards inelastic deformation of the grains themselves, particularly if the temperature is sufficiently high or the strain-rate is low. Therefore the creep of polycrystals at elevated temperatures is frequently non-uniform, because deformations caused by sliding at grain boundaries are superposed on the uniform deformations of the grains.

The mechanics of grain boundary sliding is often represented by a linearly viscous relationship between the rate of sliding and the resolved shear stress on the plane of the boundary. Ashby [1] has treated the atomistic aspects of grain boundary sliding and has derived expressions for the boundary viscosity. These derivations show that the value of the viscosity is strongly dependent on whether the angle of tilt between the crystal lattices is large or small, and on whether the tilt is symmetric. Furthermore, Raj and Ashby [2] have shown that the viscosity is strongly increased by larger irregularities, such as particles, in the grain boundary.

In a polycrystal grain boundary sliding can only take place, if a mechanism of grain deformation is available to accommodate sliding. Therefore, the rate of sliding is often determined by the rate of deformation of the grains rather than by the grain boundary viscosity. Finding the rate of sliding requires the solution of a nonlinear boundary value problem to determine the deformation fields inside the grains. Such boundary value problems have been solved numerically by Crossman and Ashby [3] and Ghahremani [4] for cases where power-law creep is the accommodating mechanism. These analyses have been carried out for plane arrays of hexagonal grains and they show a transition from a range of relatively low stresses, where grain boundary sliding gives a significant contribution to the overall strain-rate, to a range of relatively high stresses, where sliding has little effect.

Creep rupture in polycrystalline metals at high temperatures occurs mainly as intergranular fracture. Microscopic cavities nucleate and grow on the grain boundaries (Cocks and Ashby [5], Argon [6]), and coalescence of such cavities leads to micro-cracks. Experimental results show that the cavitation leading to micro-cracks occurs mainly on grain boundary facets normal to the maximum principal tensile stress direction (Hull and Rimmer [7], Trampczynski, Hayhurst and Leckie [8], Dyson, Verma and Szkopiak [9]). After that the open micro-cracks have formed, final intergranular creep fracture occurs as these cracks link up. The stress distribution in the vicinity of a cavitated facet is strongly dependent on whether or not sliding takes place at other grain boundaries adjacent to the facet. To investigate this dependence Tvergaard [10] has analysed an axisymmetric model problem, which represents a situation, where far from all the facets approximately normal to the maximum principal tensile stress are cavitated. The axisymmetric model was chosen rather than a plane model because this gives a more realistic representation of the geometric constraints in an actual three dimensional array of grains. For the same reason Anderson and Rice [11] have carried out an approximate 3-D analysis for an aggregate, in

which the grains are represented as so-called Wigner-Seitz cells. In this case all facets normal to the maximum tensile stress were taken to be cavitated. Both investigations show that grain boundary sliding has a significant influence on creep rupture. The behaviour is also very sensitive to whether or not all relevant facets are cavitated.

The final failure of a polycrystal, after that micro-cracks have been formed, can occur by grain boundary sliding accommodated by power-law creep of the grains. Axisymmetric model analyses have been carried out by Tvergaard [12], to get an estimate of the time required for this final part of the failure process.

In the present paper these different investigations of the influence of grain boundary sliding on the mechanical behaviour of materials will be discussed.

2. GRAIN BOUNDARY VISCOSITY

Grain boundaries are in some cases modelled as thin layers, which slide in a Newtonian viscous way, when a shear stress τ is applied in the plane of the boundary. The thickness δ of these layers is typically of the order of twice the atom size.

The microscopic, atomistic aspects of sliding at a boundary between two grains have been treated by Ashby [1]. During sliding atoms move by diffusion from one side of the boundary to the other, and thus sliding is accompanied by migration of the grain boundary. The viscous resistance against sliding depends on the shapes of the grain surfaces that meet at the boundary, and on the angle of tilt between the crystal lattices of the two grains.

For a symmetric high-angle boundary Ashby [1] has derived a simple expression for the boundary viscosity, relating the shear stress τ to the relative sliding velocity $\dot{u}$. In this derivation attention is focussed on the atom transport needed to preserve the structure of the boundary, while it slides. It is argued that the stress raises the chemical potential of certain atoms in one crystal (to the value μ_1) and lowers the potential of certain atoms in the other crystal (to μ_2) and that during sliding atoms flow from regions of high to regions of low potential. The power dissipated must be supplied by the external stress, so that

$$\tau \dot{u} = \dot{N}(\mu_1 - \mu_2) \qquad (2.1)$$

where $\dot{N}$ is the number of atoms flowing per unit time per unit boundary area. The flux is proportional to the gradient of the chemical potential, which gives an expression for $(\mu_1 - \mu_2)$ in terms of $\dot{N}$, and furthermore conservation of matter gives $\dot{N}$ proportional to $\dot{u}$. Substituting these two expressions into (2.1) gives

$$\tau = \eta_B \frac{\dot{u}}{\delta} \quad , \quad \eta_B = \frac{kT}{8bD_B} \qquad (2.2)$$

which defines the boundary viscosity η_B in terms of the boundary diffusion coefficient D_B, the atom size b, Boltzmann's constant k, and the absolute temperature T.

Ashby [1] also explains that in reality sliding does not occur in the continuous way suggested by the first derivation, but by the motion of appropriate boundary dislocations in the boundary plane. A derivation based on this mechanism gives the following alternative expression for the boundary viscosity

$$\eta_B = \frac{kT}{8bD_B(\rho\lambda)} \qquad (2.3)$$

where ρ is the number of dislocations per unit length, and λ is the length of the boundary periodicity. Thus, (2.3) and (2.2) are identical when ρ approaches the limit $1/\lambda$, but for low dislocation densities on the boundary the viscosity η_B is significantly higher than the lower bound (2.2).

At a low angle tilt boundary the shear viscosity is much higher [1]. Here, the cores of the dislocations that form the low angle boundary are separated by good crystal, and therefore the flow of atoms must occur by bulk diffusion, which is much slower than boundary diffusion. On the other hand, probably most real grain boundaries belong to the high-angle type, where the shear viscosity is relatively lower, because the grain boundary can act as a high-diffusivity channel.

The viscosities calculated so far are based on the assumption that irregularities on the boundary surface are of atomic height. However, boundaries are seldom as flat as this, and larger irregularities increase the viscosity. Raj and Ashby [2] have analysed the influence of various irregularities. For a periodic stepped boundary, assuming that boundary diffusion is the dominant mode of matter transport from ledge to ledge, the viscosity is raised by a factor $(h/b)^2$, when h is the height of the steps, so that the viscosity in (2.2) is increased to the value

$$\eta_B \simeq \frac{kTh^2}{8b^3D_B} \qquad (2.4)$$

A dispersion of particles or precipitates in the grain boundary raise the grain boundary viscosity in a similar manner [2,3].

3. SLIDING ACCOMMODATED BY POWER-LAW CREEP

In a polycrystalline solid sliding at the grain boundaries would lead to incompatibilities between the grains, if there was not a mechanism of grain deformation to accommodate sliding. The accommodating mechanism can be elastic deformations of the grains. For a solid subject to high temperature creep the accommodating mechanism is either dislocation creep of the grains, usually modelled as power-law creep, or diffusion (i.e. diffusional flow of matter through the grain or along its boundaries).

The effect of grain boundary sliding in a power-law creeping polycrystal has been analysed by Crossman and Ashby [3]. They considered a plane array of hexagonal grains (see Fig. 1), where

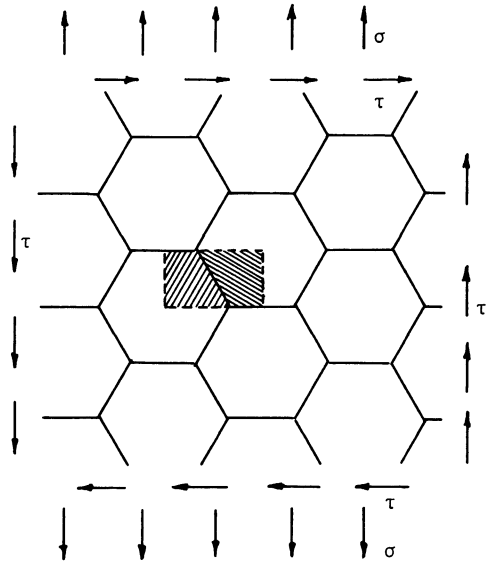

Fig. 1. Plane array of hexagonal grains. Only the hatched region is analysed.

sliding at the grain boundaries is assumed to follow a linearly viscous law of the form (2.2), with a viscosity η_B dependent on grain boundary irregularities such as particles or precipitates. The creep strain-rate tensor $\dot{\eta}^C_{ij}$ inside the grains is represented by the usual expression for lower-law creep

$$\dot{\eta}^C_{ij} = \dot{\varepsilon}^C_e \frac{3}{2} \frac{s_{ij}}{\sigma_e} \quad , \quad \dot{\varepsilon}^C_e = \dot{\varepsilon}_o \left(\frac{\sigma_e}{\sigma_o}\right)^n \qquad (3.1)$$

where $\dot{\varepsilon}_o$ and σ_o are reference strain-rate and stress quantities, the creep exponent is n, the stress deviator is $s^{ij} = \sigma^{ij} - G^{ij}\sigma^k_k/3$, expressed in terms of the stress tensor σ^{ij} and the metric tensor G^{ij}, and $\sigma_e = (3s_{ij}s^{ij}/2)^{\frac{1}{2}}$ is the effective Mises stress.

The numerical solutions in [3] were obtained by the finite element method, using a fine mesh near the triple points, where very high strain-rates occur. Also the grain boundary regions were modelled by elements, which made it necessary to give these regions an unrealistically large thickness around 1 per cent of the grain size. For high stress levels and relatively high creep strain-rates nearly no sliding was predicted at the grain boundaries, whereas for low stress levels the shear stresses at the grain boundaries were released so rapidly that there was essentially free sliding. Thus, both at low stresses and at high stresses the aggregate follows power-law creep (with different values of the reference strain-rate), whereas power-law creep is not satisfied in an intermediate stress range, where a transition occurs between the two straight lines in the $\log \dot{\varepsilon}_e$ vs. $\log \sigma_e$ diagram shown in Fig. 2.

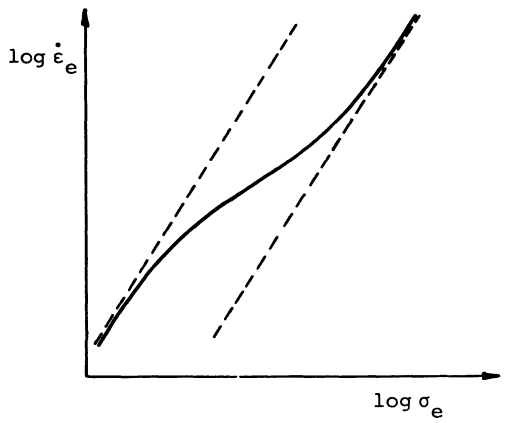

Fig. 2. Illustration of transition region due to linearly viscous sliding between power-law creeping grains.

In the low stress range, where the boundaries slide freely, the strain-rate field inside a single grain is strongly non-uniform, even though the specimen is subjected to a uniform macroscopic stress state. Since the linearly viscous behaviour in the grain boundaries has no influence here, all resistance to creep of the aggregate comes from power-law creep (3.1) inside the grains, and therefore the stress dependence of the macroscopic creep strain-rate will still follow a power-law with the same exponent n. Crossman and Ashby [3] write the expression for the macroscopic creep strain-rates in the form (3.1a), but with the effective creep strain rate $\dot{\varepsilon}^C_e$ given by a modified expression

$$\dot{\varepsilon}^C_e = \dot{\varepsilon}_o \left(f \frac{\sigma_e}{\sigma_o}\right)^n \qquad (3.2)$$

Here, the stress enhancement factor f ($f > 1$) describes the acceleration of creep caused by freely sliding boundaries. The stress enhancement factor was calculated in [3] for values of the creep exponent n of 1.0, 4.4 and 8.8, respectively, and in all three cases $f = 1.1 \pm 0.01$ was found. For pure aluminium with two different grain sizes Crossman and Ashby [3] estimated the location of the transition region as a function of stress and temperature and plotted this boundary into the deformation-mechanism maps.

Ghahremani [4] also analysed a plane array of hexagonal grains with linearly viscous grain boundary sliding accommodated by power-law creep of the grains. He found the transition from freely sliding grain boundaries, and he also calculated the stress enhancement factor f in (3.2) as a function of n. The values of f found here are somewhat higher than those found in [3], ranging from 1.16 for $n = 1$ to 1.22 for $n = 10$. In [4] the linearly viscous behaviour in the grain boundaries is represented by a jump condition, which directly relates the difference in tangential displacement rates of the grain surfaces on either side of the boundary to the shear stress on the boundary. Thus, in [4] no finite elements are used to represent the thin grain boundary layer. Ghahremani explains the discrepancy between the values of f found in [3] and [4] by the way in which the grain boundaries are modelled. The elements inside a thin boundary layer must have very large aspect ratios, and it is known that such large aspect ratios tend to reduce the accuracy of the solution.

An early work describing the effect of linear viscous sliding in the boundaries between power-law creeping grains is that of Hart [13], which makes use of simple fiber models to develop a phenomenological model. Although these fiber models do not account for the details of the polycrystal deformation, Hart did predict the transition range and the limiting power-law behaviour at low and high stresses, respectively.

Elastic accommodation of grain boundary sliding can play a role when a polycrystalline material is subjected to cyclic loading, while the stress levels remain so low that power-law creep has no influence. In such circumstances sliding at the boundaries leads to a reduction of the elastic moduli, and the grain boundary viscosity contributes to the dissipation of mechanical energy into heat. These effects of sliding can be represented in terms of the complex viscoelastic moduli of the material. A numerical analysis of the complex shear modulus has been carried out by Ghahremani [14], for a model material made up of a plane array of hexagonal grains, as that shown in Fig. 1. This analysis has resulted in curves showing the real and imaginary parts of the shear modulus as functions of the frequency of oscillation, the elastic modulus of the grains, the grain size and the grain boundary viscosity.

The accommodation of sliding discussed in the present section relates to the deformations of a whole grain necessary to allow for sliding. However, it is noted that, for a non-planar boundary, also the derivation of the grain boundary viscosity itself (e.g. see (2.4)), depends on local deformations necessary to accommodate sliding [1,2]. Thus, the rate of sliding depends on various accommodating mechanisms, which are active on quite different size scales.

4. EFFECT OF SLIDING ON CREEP RUPTURE

Creep rupture in polycrystalline metals at elevated temperatures can occur by a number of different mechanisms. Ashby and Dyson [15] have distinguished four broad categories of failure mechanisms, i.e. loss of cross-sectional area associated with large strain, failure by the formation and subsequent growth of cavities, accelerated creep due to degradation of the microstructure, or damage by gas-environmental attack. Here, the focus will be on material models that consider the growth of cavities on grain boundary facets roughly perpendicular to the maximum principal tensile stress direction. This type of intergranular damage, belonging to the second category discussed in [15], is frequently observed in experiments.

For a case with no grain boundary sliding Rice [16] has suggested modelling a cavitating facet as a penny-shaped crack, where the normal tensile stress σ_n necessary for cavity growth acts on the crack surfaces. A constitutive model for creep with grain boundary cavitation has been developed by Tvergaard [17] as an extension of this penny-shaped crack model, making also use of an expression for the macroscopic creep strain rate of a micro-cracked solid, derived by Hutchinson [18].

When sliding takes place at the grain boundaries adjacent to a cavitating grain boundary facet, this facet cannot directly be modelled as a penny-shaped crack. Some insight in the effect of sliding on grain boundary cavitation can be gained from the numerical solution of model problems, such as the axisymmetric model studied by Tvergaard [10]. This model is illustrated in Fig. 3. The maximum

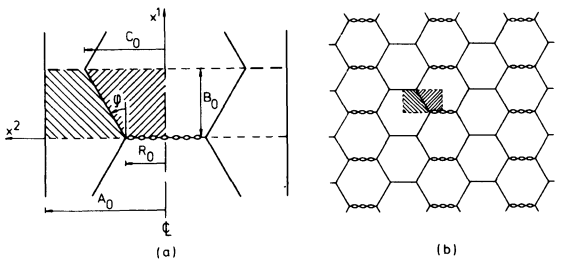

Fig. 3. Axisymmetric model problem used to study the influence of sliding on grain boundary cavitation. Only the hatched region is analysed.

principal tensile stress is in the x^1-direction, normal to the cavitated facet. Half of each grain adjacent to this facet is represented by a truncated cone emanating from the edges of the facet, while the external ring of material represents part of a number of grains surrounding the two central grains of the model.

Only completely free grain boundary sliding is accounted for in the analyses in [10]. Thus, the grain boundary viscosity η_B in (2.2) is considered negligible, which means that the model refers to the behaviour at relatively low stress levels, below a transition range analogous to that illustrated in Fig. 2.

The type of periodicity of the cavitated facets implied by the axisymmetric model is shown in Fig. 3b, which illustrates that not all facets normal to the maximum principal tensile stress are taken to be cavitated. In cases, where the normal tractions on the cavitating facets are essentially zero, a significant part of the load is carried through the uncavitated facets, whereas with all relevant facets cavitated the full load would have to be carried through sliding facets inclined to the tensile direction. The model in Fig. 3, with zero sliding at the triple points where no facets are cavitated, is expected to also give a good indication of the cavitation behaviour in cases where fewer facets are cavitated. However, if significantly more facets are cavitated than shown in Fig. 3b, the present model would no longer give a good approximation.

The material inside the grain is taken to deform by power law creep (3.1) in addition to elastic deformations. The freely sliding behaviour at the grain boundaries is described approximately in terms of a layer of linear elastic springs. Thus, tangential stresses on the sliding surfaces are neglected, and the true stress σ_n normal to the current orientation of the grain boundary is taken to be

$$\sigma_n = k\,d \tag{4.1}$$

where k is the spring stiffness, and d is the distance between the two grains sliding against one another. Allowing for a non-zero distance d gives an inaccuracy, which is kept very small by using a large stiffness k.

At time $t = 0$ the loads are applied at the surface of the model in Fig. 3a, and subsequently the loads vary slightly with time, such that the values of the average axial and radial true stresses σ_1 and σ_2 remain fixed. The deformations of the grains are approximated by finite elements, using the mesh shown in Fig. 4, and large strains are accounted for in the analysis.

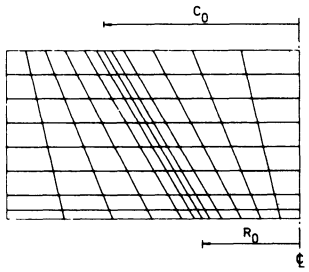

Fig. 4. Finite element mesh used in numerical analyses.

The details of the field equations and the boundary conditions are specified in [10] and shall not be repeated here.

The grain boundary cavities, with average spacing $2b$ and radius a, grow by diffusion as well as by dislocation creep of the surrounding material. The diffusion along the void surface is assumed to be sufficiently rapid, relative to the diffusion along the grain boundary, to maintain the quasiequilibrium spherical-caps void shape (see Fig. 5). At sufficiently low tensile stresses cavity growth by grain boundary diffusion is dominant. Then the rate of growth of the cavity volume is obtained by the rigid grains model, early analysed by Hull and Rimmer [7], and subsequently modified by various authors, including Needleman and Rice [19], who found

$$\dot{V}_1 = 4\pi\,\mathcal{D}\,\frac{\sigma_n - (1-f)\sigma_s}{\ell n(1/f) - (3-f)(1-f)/2} \tag{4.2}$$

Here, σ_n is the average normal stress on the facet in the vicinity of the cavity, σ_s is the sintering stress, f is the area fraction of the

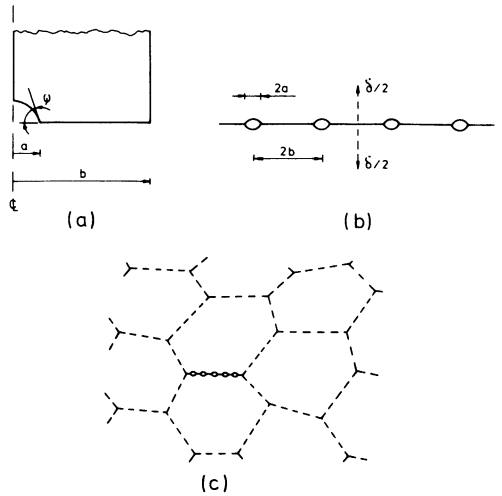

Fig. 5. (a) Spherical-caps shape of a single cavity. (b) Equally spaced cavities on a grain boundary. (c) An isolated, cavitated grain boundary facet in a polycrystal.

grain boundary which is cavitated, and $\mathcal{D} = D_B\delta_B\Omega/kT$ is the grain boundary diffusion parameter, where $D_B\delta_B$ is the boundary diffusivity, and Ω is the atomic volume.

Based on approximate results by Budiansky, Hutchinson and Slutsky [20], for the growth of a spherical void in a power-law creeping material, the following volumetric growth-rate expressions relating to the spherical-caps shape are employed

$$\dot{V}_2 = \begin{cases} \pm 2\pi\dot{\varepsilon}_e^C a^3 h(\psi)\left[\alpha_n\left|\frac{\sigma_m}{\sigma_e}\right| + \beta_n\right]^n & \text{, for } \pm\frac{\sigma_m}{\sigma_e} > 1 \\ 2\pi\dot{\varepsilon}_e^C a^3 h(\psi)[\alpha_n + \beta_n]^n \frac{\sigma_m}{\sigma_e} & \text{, for } \left|\frac{\sigma_m}{\sigma_e}\right| \leq 1 \end{cases} \tag{4.3}$$

Here, $\dot{\varepsilon}_e^C = \dot{\varepsilon}_o(\sigma_e/\sigma_o)^n$ is the effective creep strain-rate, σ_m and σ_e are the mean stress and Mises stress, respectively, representing the average stress state in the vicinity of the void, and the constants are given by $\alpha_n = 3/2n$, $\beta_n = (n-1)(n+0.4319)n^2$ and $h(\psi) = [(1+\cos\psi)^{-1} - \cos\psi/2]/\sin\psi$. For the high triaxiality range, $\sigma_m/\sigma_e > 1$, the expression (4.3) was suggested by Sham and Needleman [21], and the Low triaxiality approximation was introduced in [22].

Needleman and Rice [19] have used the parameter

$$L = (\mathcal{D}\sigma_e/\dot{\varepsilon}_e^C)^{1/3} \tag{4.4}$$

as a stress and temperature dependent length scale, where $\mathcal{D}$, σ_e and $\dot{\varepsilon}_e^C$ are the values appearing in (4.2) and (4.3). Thus, for $a/L < 0.1$ the total volumetric growth-rate of a cavity with radius a is very well approximated by (4.2), whereas growth-rates larger than that predicted by (4.2) are found for higher values of a/L, due to an increasing influence of dislocation creep.

The following approximation of the cavity growth-rate

$$\dot{V} = \dot{V}_1 + \dot{V}_2 \quad \text{, for } \frac{a}{L} \leq 10 \text{ ,}$$
$$f = \max\left\{\left(\frac{a}{b}\right)^2 , \left(\frac{a}{a+1.5L}\right)^2\right\} \tag{4.5}$$

taking into account the interaction of diffusive growth and power-law creep growth, has been found to agree with numerically determined growth-rates, both for the high triaxiality range [21], and for lower triaxialities [19,22]. From (4.5) the rate of growth of the cavity radius is found as $\dot{a} = \dot{V}/(4\pi a^2 h(\psi))$.

The average separation between the two grains adjacent to the cavitating facet is $\delta = V/\pi b^2$, where V is the cavity volume and $2b$ is the average spacing. Thus the rate of growth of this separation, $\dot{\delta}$, to be used as boundary condition in the model problem (Fig. 3a), is given by

$$\dot{\delta} = \frac{\dot{V}}{\pi b^2} - \frac{2V}{\pi b^2}\frac{\dot{b}}{b} \tag{4.6}$$

Many metals appear to contain rather few cavities in the initial stages of creep, so that the time required for the nucleation of new cavities may have a significant effect on the total rupture time. Different mechanisms of cavity nucleation, discussed by Argon [6] and Dyson [23], have the common feature that they depend on dislocation creep, which is a stochastic process, and this can explain why nucleation is often found to occur continuously during creep. Some experimental investigations indicate that the number of cavities is proportional to the effective strain, so that the rate of increase of the cavity number N per unit initial area of the grain boundary facet is given by

$$\dot{N} = \frac{dN}{d\varepsilon_e}\dot{\varepsilon}_e \quad , \quad \frac{dN}{d\varepsilon_e} = \text{constant} \tag{4.7}$$

In some cases continuous nucleation is observed until fracture, whereas in other cases a saturation value N_{max} is reached before rupture [23].

Now, the simplifying assumptions are used that all cavities near a given point of the facet are of equal size (equal to the size of the cavity first nucleated at that point) and equally spaced. In principle, the growth of cavities nucleated at different times should be followed separately; but small voids grow much faster than larger voids, due to diffusion, and analyses indicate that the smaller voids catch up so rapidly that neglecting the size differences may be a good approximation. Then, with $\dot{N}$ given by (4.7), the ratio $\dot{b}/b$, to be substituted into (4.6) is simply taken to be

$$\frac{\dot{b}}{b} = \frac{1}{2}\left(\frac{\dot{\lambda}_I}{\lambda_I} + \frac{\dot{\lambda}_{II}}{\lambda_{II}}\right) - \frac{1}{2}\frac{\dot{N}}{N} \tag{4.8}$$

where λ_I and λ_{II} are the principal stretches at the point considered on the facet.

In the numerical solution the stresses σ_m and σ_e in the expression (4.3) were calculated as averages over the four triangular elements within each quadrilateral in the row of elements adjacent to the grain boundary facet. The normal stress σ_n in (4.2) could be obtained the same way; but the expression (4.1) was preferred, to better represent the variation of σ_n near the triple grain junction (at $x^2 = R_0$). For the sintering stress σ_s in (4.1) the value $\sigma_s = 0$ was used as an approximation.

The geometry of the model problem used for the results presented in the next few figures is given by $B_0/A_0 = 0.577$, $R_0/A_0 = 0.333$ and $C_0/A_0 = 0.667$, so that the cone angle is $\phi = 30^o$ (see Fig. 3a). The creep exponent is taken to be $n = 5$, Poisson's ratio is $\nu = 1/3$ and the angle defining the spherical-caps shape of the cavities (Fig. 5) is taken to be $\psi = 75^o$. The figures show the growth of a/b as a function of time at the two radii $x^2/R_0 = 0.20$ and $x^2/R_0 = 0.92$,

and coalescence of the cavities is taken to occur when a/b is close to unity. All times are normalized by a reference time $t_R = \sigma_e/(E\dot{\varepsilon}_e^C)$, where $\sigma_e = |\sigma_1 - \sigma_2|$ is the average effective Mises stress and $\dot{\varepsilon}_e = \dot{\varepsilon}_o(\sigma_e/\sigma_o)^n$ is the corresponding effective creep strain-rate.

The average true stresses, relative to Young's modulus E, are specified by $\sigma_1/E = 0.001$ and $\sigma_2/\sigma_1 = 0.5$, so that the average effective Mises stress is $\sigma_e/E = 0.0005$. All cavities are assumed to be present from the beginning, uniformly distributed over the facet and of equal size, specified by the initial values $a_I/b_I = 0.1$ and $b_I/R_0 = 0.1$. The grain boundary diffusion parameter $\mathcal{D}$ is given in terms of L by the initial value $a_I/L_I = 0.025$ (based on substituting the average macroscopic values of σ_e and $\dot{\varepsilon}_e^C$ into (4.4)).

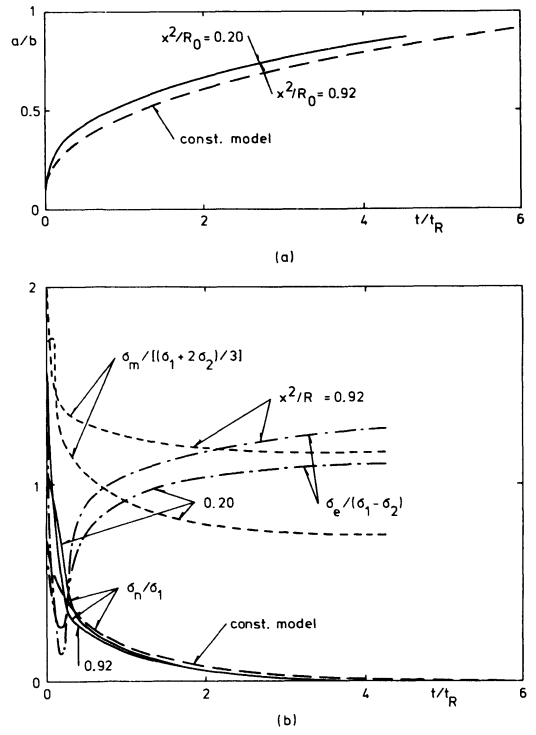

Fig. 6. Development of cavities and stresses at a grain boundary facet for $a_I/L_I = 0.025$ (from [10]).

Fig. 6a shows that the rate of growth of the cavities near the edge of the facet is nearly identical to that near the centre, in contrast to the result found in the absence of grain boundary sliding, where the cavity growth is slower near the edge [22]. This uniform opening of the facet is also seen in the deformed meshes shown in Fig. 7. Furthermore, the cavity growth found in Fig. 6a is about six times as fast as that found without sliding [22], so sliding has a very significant effect on the time to failure by cavity coalescence. The constitutive model referred to in the figures will be discussed subsequently, in Section 5.

Fig. 6b shows that the normal stresses σ_n on the cavitating facet decay rapidly towards zero, because the power law creep of the grains is not rapid enough to accommodate the diffusive cavity growth-rate (4.2) that would occur under a higher normal stress. This situation, first noted by Dyson [24], is usually described as creep constrained

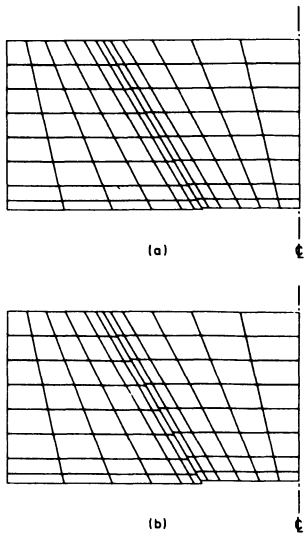

Fig. 7. Deformed meshes corresponding to $a_I/L_I = 0.025$. (a) $t/t_R = 2.21$, (b) $t/t_R = 4.27$ (from [10]).

cavitation. A characteristic feature associated with creep constrained cavitation is that failure occurs at relatively small strains.

Figs. 8 and 9 show the results of a computation, where the only difference from that illustrated above is a smaller value of the grain boundary diffusion parameter specified by $a_I/L_I = 0.33$.

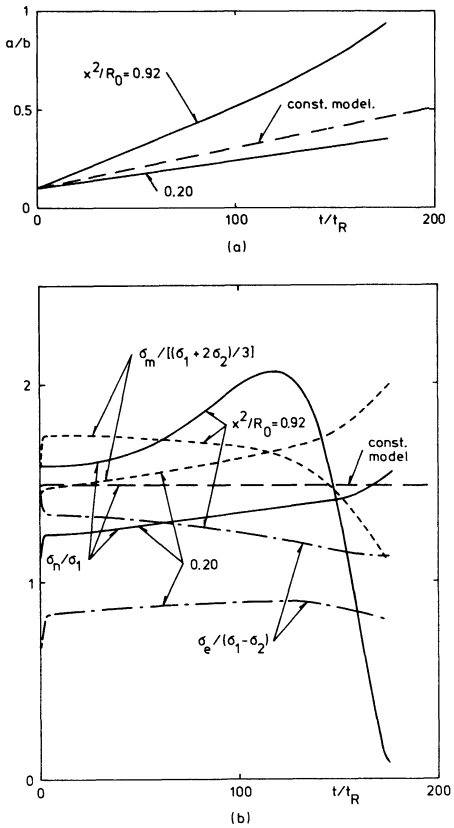

Fig. 8. Development of cavities and stresses at a grain boundary facet for $a_I/L_I = 0.33$ (from [10]).

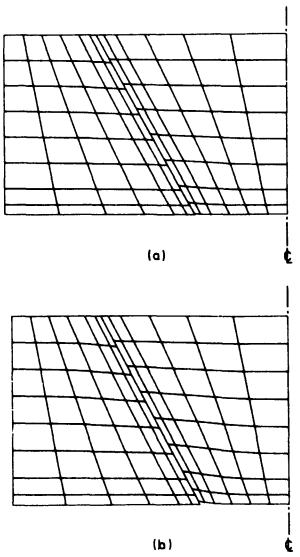

Fig. 9. Deformed meshes corresponding to $a_I/L_I = 0.33$. (a) $t/t_R = 87.1$. (b) $t/t_R = 152$ (from [10]).

Here, the normal stress is not relaxed before final failure occurs, and thus the cavity growth is not creep constrained. Fig. 8a shows that in this case grain boundary sliding results in much faster growth near the edge of the facet than in the central part of the facet. This behaviour is also clearly visible in the deformed meshes in Fig. 9, which show the formation of wedge-cracks by early cavity coalescence at triple point junctions. It is also noted that the strains are much larger here than those found in the previous case, e.g. the logarithmic strain $\varepsilon_1 = 0.115$ at $t/t_R = 152$. The initial failure at the triple point in Fig. 8 occurs at about 1/4 of the time to failure in the absence of grain boundary sliding.

Several other cases have been analysed in [10], and in general these results confirm the types of response shown in Figs. 6 - 9. This is also true when continuous nucleation of cavities takes place during the lifetime, as modelled by (4.7) and (4.8). However, in a case corresponding to that considered in Figs. 6 and 7, the relaxation of σ_n to creep constrained cavitation is somewhat delayed when all cavities are not yet nucleated and the macroscopic logarithmic strain at failure is somewhat increased.

The interaction of free grain boundary sliding and intergranular cavitation has also been analysed by Anderson and Rice [11], who represented the grains by so-called Wigner-Seitz cells. For such grain shapes a full 3D analysis is required, and this is done approximately in [11] by application of a stress-based variational principle. A significant difference from the type of situation illustrated in Fig. 3b is that Anderson and Rice [11] consider the limiting case, where all facets normal to the maximum tensile stress are cavitated. This does not give too large differences in a range with no creep constraint on cavitation (such as Figs. 8 and 9); but in the creep constrained range, where $\sigma_n \simeq 0$ on the cavitating facets, it has the drastic effect that the macroscopic creep rates are increased by a factor 100 or more.

When open microcracks have formed by cavity coalescence on a number of grain boundary facets, final failure requires that these microcracks link up. This final failure process can occur by cavity growth on adjacent grain boundaries inclined to the maximum tensile stress direction, by a mechanism that mainly relies on the opening of the microcracks due to grain boundary sliding, or by a combination of these mechanisms. The grain boundary sliding mechanism of final failure has been investigated by Tvergaard [12], in terms of analyses for axisymmetric model problems with an initial geometry as that shown in Fig. 3a. Various sets of boundary conditions have been employed in an attempt to model different microcrack densities, within the context of the relatively simple axisymmetric model problem. These boundary conditions shall not be explained here.

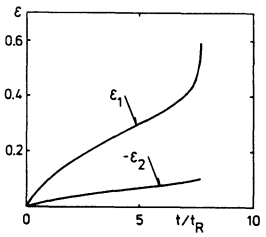

Fig. 10. Average logarithmic strains vs. time during final failure by grain boundary sliding (from [12]).

For one of the cases analysed Fig. 10 shows the development of the macroscopic logarithmic strains ε_1 and ε_2 in the axial and radial directions, respectively, when $\sigma_2/\sigma_1 = 0.5$, and Fig. 11 shows

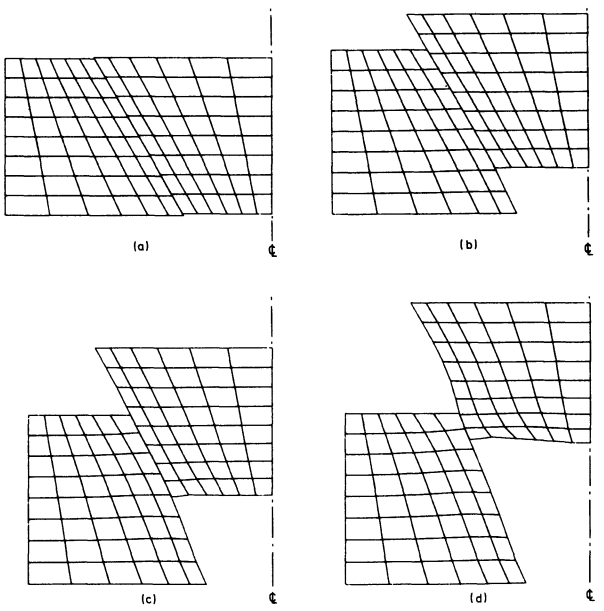

Fig. 11. Deformed meshes during final failure by grain boundary sliding. (a) $\varepsilon_1 = 0.010$. (b) $\varepsilon_1 = 0.245$. (c) $\varepsilon_1 = 0.414$. (d) $\varepsilon_1 = 0.586$ (from [12]).

the corresponding deformed meshes at four stages of the computation. Based on a number of computations of this type it was concluded in [12] that the final separation by sliding may take a significant part of the lifetime, particularly if the microcracks are rather sparse. It is also noted that separation by sliding is most likely to be dominant if the relevant value of a_I/L_I is

relatively large.

In the early stages, some of the cases analysed in [12] can be considered analogous to creep constrained cavitation with all relevant facets cavitated. It is noted that the very high overall creep rates found in these cases confirm the high creep rates found by Anderson and Rice [11] for similar cases.

It should be emphasized that a plane strain model analogous to the axisymmetric model studied in [12] would give quite different results. For a planar, hexagonal array of grains (Fig. 1), with microcracks formed at all grain facets normal to the maximum tensile stress, and with free sliding at the remaining grain boundaries, separation by sliding would occur immediately without any deformation of the grains. The main reason for considering grains in the form of truncated cones [10,12] or Wigner Seitz cells [11], is that these models require an accommodating deformation mechanism rather similar to that needed in an actual three-dimensional array of grains.

5. APPROXIMATE CONSTITUTIVE EQUATIONS

The constitutive equations proposed by Tvergaard [17] for a material subject to creep and grain boundary cavitation are an extension of work by Rice [16] and Hutchinson [18]. These investigations rely on treating cavitating facets as penny-shaped cracks in a power-law creeping material, and therefore the model does not account for the effect of sliding on grain boundaries adjacent to the cavitating facets. However, some relatively simple modifications of this material model can give a reasonable approximation of the sliding effects [10].

Rice [16] has already suggested modifications of his creep constrained cavitation model, based on equilibrium considerations for a planar, hexagonal array of grains with freely sliding grain boundaries. Furthermore, he suggested that the inclined sliding grain boundaries would act as an increased effective radius of the cavitating facet, which is equivalent to an increased rate of opening of the micro-crack. The considerations in [16] for uniaxial tension are easily generalized to a planar, hexagonal array of grains subject to a multi-axial stress state. However, the grains in an actual three-dimensional array are more constrained geometrically than the grains in a plane array, and such stronger geometric constraints are represented by the axisymmetric model Fig. 3a considered in [10].

The modifications of the constitutive model are guided partly by the proposals of Rice [16], and partly by the stress distributions and crack opening rates found in [10]. The macroscopic maximum principal tensile stress in the direction normal to the cavitating facet is denoted by S and the components of a tensor m_{ij} are defined so that $S = \sigma^{ij} m_{ij}$ (i.e. $m_{ij} = \bar{n}_i \bar{n}_j$ where $\bar{n}_i$ is the facet normal in the current configuration). Now, a constant c_1 is introduced to define two alternative stress measures

$$S^* = S + \frac{3}{2} c_1 (S - \sigma_m)$$
$$\sigma_m^* = \sigma_m + \frac{3}{2} c_1 (S - \sigma_m) \qquad (5.1)$$

where $\sigma_m = \sigma_k^k/3$ is the macroscopic mean stress, so that $S^* = \sigma^{ij} m_{ij}^*$ for $m_{ij}^* = m_{ij} + c_1(3m_{ij} - G_{ij})/2$. The stress measures S^* and σ_m^* are assumed to represent the normal stress and the mean stress, respectively, at a facet that is not subject to cavitation, and thus the local Mises stress $\sigma_e^* = \sigma_e$ is assumed unaffected by sliding. It is noted that (5.1a) can also be expressed in terms of the stress deviator tensor s^{ij}, as

$$S^* = s^{ij} m_{ij} \left(1 + \frac{3}{2} c_1\right) + \sigma_m \qquad (5.2)$$

which reflects the fact that neither creep nor grain boundary sliding of a polycrystal are affected by changes in the mean stress σ_m, but that the normal stress S^* on the facet changes with σ_m.

The behaviour of a cavitating facet in a material with free grain boundary sliding is now approximated by the expression corresponding to no sliding, but for a crack subject to the modified macroscopic principal stress values. Also, the rate of opening of the crack is taken to be higher, for which purpose another constant c_2 is introduced, to increase the amplitude of the rate of crack opening expression

$$\beta^* = c_2 \beta \quad , \quad \rho^* = c_2 \rho \qquad (5.3)$$

Then, the average rate of opening of the crack, representing the cavitating facet, is approximated by the expression

$$\dot{\delta} = \beta^* \frac{S^* - \sigma_n^*}{\sigma_e} \dot{\varepsilon}_e^C 2R \qquad (5.4)$$

where R is the current radius of the facet. For the value of β, corresponding to a penny-shaped crack, He and Hutchinson [25] have found the following asymptotic expression

$$\beta \simeq \frac{4}{\pi}\left(1 + \frac{3}{n}\right)^{-\frac{1}{2}} \qquad (5.5)$$

which is highly accurate for all n for $|S^*/\sigma_e^*| \leq 2$, but inaccurate in the high triaxiality range for S^*/σ_e^* larger than about 3 or 4.

The average normal stress σ_n^* on the facet is determined such that (5.4) is equal to (4.6) for an average cavity, where the expressions (4.2) and (4.3) for the volumetric growth-rates are based on the modified stress values.

The modification of the expression (5.4) for the rate of opening of a facet should also be incorporated in the expression for the macroscopic creep strain rates used by Tvergaard [17]. Since this expression is based on the results of Hutchinson [18] and He and Hutchinson [25], the modified expression is

$$\dot{\varepsilon}_{ij}^C = \dot{\varepsilon}_o \left(\frac{\sigma_e}{\sigma_o}\right)^n \left[\frac{3}{2} \frac{s_{ij}}{\sigma_e}(1 + \gamma) + \rho^* \left\{\frac{3}{2} \frac{n-1}{n+1} \frac{s_{ij}}{\sigma_e} \left(\frac{S^* - \sigma_n^*}{\sigma_e}\right)^2 + \frac{2}{n+1} \frac{S^* - \sigma_n^*}{\sigma_e} m_{ij}^* \right\}\right] \qquad (5.6)$$

where ρ^* is given by (5.3b). The factor ρ reflects the density of cavitating facets, and Hutchinson [18] found

$$\rho = 4R^3 \Lambda (n+1) \left(1 + \frac{3}{n}\right)^{-\frac{1}{2}} \qquad (5.7)$$

Here, R is the radius of the penny-shaped cracks, and Λ is the number of cracks per unit volume.

Even in cases with no cavitation (i.e. $\dot{\delta} = 0$ in (5.4) and thus $\sigma_n^* = S^*$) the free grain boundary sliding adds to the macroscopic creep strain-rates, without affecting incompressibility. This is analogous to the behaviour discussed in Section 3 of this paper [3,4], where essentially free sliding adds to the creep rate at stress levels below the transition range. In (5.6) this effect is represented by the parameter γ whereas in

(3.2) the stress enhancement factor f is used. It has been found in [10], for $n = 5$, that $\gamma = 0.5$ gives a good approximation of the numerical results. Ghahremani [4] found a somewhat stronger effect of free grain boundary sliding for $n = 5$; but this was to be expected, since the axisymmetric grains are more geometrically constrained against sliding than the planar hexagonal grains studied in [4].

It is noted that for $c_1 = 0$, $c_2 = 1$ and $\gamma = 0$ the material description based on (5.4) and (5.6) reduces to that obtained without grain boundary sliding [17]. The numerical model studies with free sliding in [10], representing well-separated cavitating facets, are reasonably well approximated by taking $c_1 = 1$, $c_2 = 4$ and $\gamma = 0.5$. The type of approximation obtained by this set of parameters is illustrated by the curves marked constitutive model in Figs. 6 and 8. As already discussed in Section 4 cavitation on all facets normal to the maximum tensile stress gives very strongly increased overall strain rates. Overall creep rates of the order of magnitude of those found in [11] for closely-spaced cavitating facets are obtained by using $c_1 = 1$, $c_2 = 200$ and $\gamma = 0.5$ (taking $\rho \simeq 0.75$ for $n = 5$).

The effect of multi-axial stress states on the creep rupture times predicted by the material model can be illustrated by drawing curves through points in stress space that all correspond to a given rupture time. Most experimental investigations have considered plane stress states, and Hayhurst [26] has drawn isochronous rupture loci based on a number of such tests, comparing them with predictions of continuum damage mechanics. For comparison with such experimental curves Tvergaard [27] has plotted a number of predictions of the material model considered in the present section.

Plane stress isochronous rupture loci are shown in Fig. 12 for three cases, in which the initial

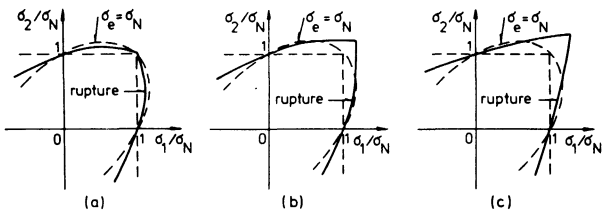

Fig. 12. Isochronous rupture loci for plane stress, $\sigma_3 = 0$. (a) No sliding. (b) Sliding with well-separated cavitating facets. (c) Sliding with closely-spaced cavitating facets (from [27]).

cavity distribution and the value of the diffusion parameter are the same, specified by $a_I/b_I = 0.1$, $b_I/R_I = 0.1$ and $a_I/L_N = 0.1$ (where L_N is a nominal value, which appears by taking σ_e equal to the nominal stress σ_N in (4.4)). It is seen that in Fig. 12a, where there is no grain boundary sliding ($c_1 = 0$, $c_2 = 1$, $\gamma = 0$), the isochronous rupture loci (solid curve) are located between the Mises ellipse and the lines of constant maximum tensile stress. The results in Fig. 12b and c correspond to freely sliding grain boundaries, for well-separated cavitating facets ($c_1 = 1$, $c_2 = 4$, $\gamma = 0.5$) and for closely-spaced cavitating facets ($c_1 = 1$, $c_2 = 200$, $\gamma = 0.5$), respectively.

In equal biaxial tension, $\sigma_1 = \sigma_2$, the results found for grain boundary sliding in Fig. 12 are rather different from those corresponding to no sliding, since with sliding a stress level significantly higher than σ_N is required to predict the same rupture time. The different experimental results mentioned in [27] seem to agree better with the shape of the rupture curve shown in Fig. 12a than with the two other curves. However, it is clear that also other models taking into account grain boundary sliding predict relatively larger lifetime in equal biaxial tension than in uniaxial tension. Thus, Anderson and Rice [11] would find the same type of dependence, with $c_1 = 0.67$ in their alternative expression for the rate of separation between two grains of a Wigner-Seitz cell geometry. Also Cocks and Ashby [5] have found rupture loci with shapes rather similar to that in Fig. 12c, based on a model of grain boundary sliding and purely diffusive cavity growth in a planar array of grains. In conclusion, it appears that isochronous rupture loci with an increased stress level in biaxial tension should be expected if there is free or nearly free grain boundary sliding.

REFERENCES

[1] ASHBY, M.F., Surface Sci. 31 (1972) 498.
[2] RAJ, R. and ASHBY, M.F., Met. Trans. 2 (1971) 1113.
[3] CROSSMAN, F.W. and ASHBY, M.F., Acta Met. 23 (1975) 425.
[4] GHAHREMANI, F., Int. J. Solids Structures 16 (1980) 847.
[5] COCKS, A.C.F. and ASHBY, M.F., Prog. Mater. Sci. 27 (1982) 189.
[6] ARGON, A.S., "Recent Advances in Creep and Fracture of Engineering Materials", (eds. B. Wilshire and D.R.J. Owen), 1, Pinerage Press, Swansea, (1982).
[7] HULL, D. and RIMMER, D.E., Phil. Mag. 4 (1959) 673.
[8] TRAMPCZYNSKI, W.A., HAYHURST, D.R. and LECKIE, F.A., J. Mech. Phys. Solids 29 (1981) 353.
[9] DYSON, B.F., VERMA, A.K. and SZKOPIAK, Z.C., Acta Met. 29 (1981) 1573.
[10] TVERGAARD, V., J. Mech. Phys. Solids 33 (1985) 447.
[11] ANDERSON, P.M. and RICE, J.R., Acta Met. 33 (1985) 409.
[12] TVERGAARD, V., Int. J. Solids Structures 21 (1985) 279.
[13] HART, E.W., Acta Met. 15 (1967) 1545.
[14] GHAHREMANI, F., Int. J. Solids Structures 16 (1980) 825.
[15] ASHBY, M.F. and DYSON, B.F., Creep Damage Mechanics and Micromechanisms, National Physical Laboratory, Report DMA(A) 77 (1984).
[16] RICE, J.R., Acta Met. 29 (1981) 675.
[17] TVERGAARD, V., Acta Met. 32 (1984) 1977.
[18] HUTCHINSON, J.W., Acta Met. 31 (1983) 1079.
[19] NEEDLEMAN, A. and RICE, J.R., Acta Met. 28 (1980) 1315.
[20] BUDIANSKY, B., HUTCHINSON, J.W. and SLUTSKY, S., "Mechanics of Solids", The Rodney Hill 60th Anniversary Volume (eds. H.G. Hopkins and M.J. Sewell), 13, Pergamon Press, Oxford (1982).
[21] SHAM, T.-L. and NEEDLEMAN, A., Acta Met. 31 (1983) 919.
[22] TVERGAARD, V., J. Mech. Phys. Solids 32 (1984) 373.
[23] DYSON, B.F., Scripta Met. 17 (1983) 31.
[24] DYSON, B.F., Metal Sci. 10 (1976) 349.
[25] HE, M.Y. and HUTCHINSON, J.W., J. Appl. Mech. 48 (1981) 830.

[26] HAYHURST, D.R., J. Mech. Phys. Solids 20 (1972) 381.

[27] TVERGAARD, V., Acta Met. 34 (1986) 243.